

Electron distributions in nonlinear Compton scattering

Madalina Boca,* Victor Dinu, and Viorica Florescu

*Department of Physics and Centre for Advanced Quantum Physics,
University of Bucharest, MG-11, Bucharest-Măgurele, 077125 Romania*

Abstract

Based on quantum theory, we investigate the distribution of the electrons scattered in nonlinear Compton effect by an electromagnetic plane wave. The monochromatic case, examined in detail, reveals features of the electron distribution, useful in the understanding of the pulsed plane wave case for particular intensity and electron energy regimes. The graphs displayed focus on the case of head-on or near head-on collision of an energetic electron with an electromagnetic circularly polarized pulsed plane wave and show that the deviation in direction is extremely small, while the distribution in energy can be visibly different from that of the initial electron. Two pulse shapes, several laser intensities and high incident electron energies are considered.

PACS numbers: 12.20.Ds, 32.80.Wr

*Electronic address: madalina.boca@g.unibuc.ro

I. INTRODUCTION

Nonlinear Compton scattering (NLCS) is one of the simplest processes predicted by quantum theory [1–3] and was detected in the head-on collision of an energetic electron beam with an intense laser beam [4, 5].

In the case of a pulsed electromagnetic plane wave (a plane wave with a finite extension in the direction of propagation), the model we use for the laser beam, an electron distribution at the end of the pulse different from the initial one can not be predicted within classical electrodynamics (CED) without including the radiation reaction (RR) as, according to this theory, the pulse leaves each electron with the same momentum it had at the beginning of the pulse. On the contrary, the emission of radiation can be described by CED as Thomson scattering: the charged particle accelerated by the electromagnetic field emits radiation during its well determined motion. The inclusion of RR in CED takes into account the energy lost by the electron and leads to a final electron momentum different of the initial one. The classical description of RR was analyzed in several publications in which not only the formalism was discussed but also the effects of radiation reaction on Thomson scattering (references can be found in the very recent review [6]). In quantum theory RR was considered only very recently [7],[8]. It is argued that the standard description of NLCS, as a single one-photon emission, using the Volkov solutions of Dirac equation, does not include radiation reaction and that the mechanism for it is the incoherent multiple one-photon emission by the electron.

Up to now comparisons between quantum and classical predictions were done only for the emitted radiation spectrum. In the work presented in this paper we do not include RR effects.

In *quantum theory* NLCS is described as the *spontaneous emission of one photon* by the electron interacting with an intense external electromagnetic field. The electromagnetic field is described classically, an approximation which is justified for high intensity; the most used model until recently was the monochromatic plane wave. The theoretical studies published in the last three years adopt a more realistic description of short pulses, the pulsed plane wave model, for NLCS [9–13] as well for other processes [14, 15]. The finite transverse extension of a real laser beam is neglected in quantum calculations, where an adequate treatment of this aspect was not developed up to now. On the contrary, in calculations based on CED,

where it is possible to include any shape of the electromagnetic field, beam size effects have been already considered [16, 17].

From a predicted probability distribution for the simultaneous detection of the emitted photon and the scattered electron, quantum theory extracts separate information on the emitted radiation, to which the majority of the results in the literature refer, or on the electron distribution, less studied up to now. It was remarked [10] that in experiments the radiation emitted in NLCS was not investigated, contrary to the Thomson case where the angular distribution of first several harmonics has been recorded [18]. Electrons have been detected in the E-144 experiment at SLAC performed 15 years ago: the collision of a 46.6 GeV electron beam with terawatt pulses from a Nd:glass laser at 1054 and 527 nm wavelengths. Comparison with the theoretical energy spectra presented in Fig. 4 of [4] reveals the absorption of up to four laser photons. More than that, a supplementary evidence was given by the detection of positrons [5] which come from a succession of two elementary processes: NLCS, and (e^-, e^+) pair creation by the energetic photon emitted in the first process.

In the monochromatic case, the electron energy distribution presents thresholds [4, 5] that can be connected with the absorption of fixed number of laser photons; these thresholds will be discussed in Sect. III.

In connection with the perspective of very intense sources of radiation [19], the interest of studying NLCS along with other processes in the very intense regime (intensities above 10^{22} W/cm²) has increased and it is reflected in the most recent works [20]. Theoretical aspects as the use of a wave packet for the description of the initial electron [21] or the quantum description of the external electromagnetic field are reanalyzed [22].

Our paper is a theoretical study of the *electron distribution in NLCS* occurring in the interaction of the electron with a laser pulse. We have recently published a few results from a preliminary investigation of this distribution [23]. The present paper is organized as follows. Section II displays the general expression of the multiple differential distribution describing both photons and electrons, from which analytic expressions for the electron distribution in the monochromatic or pulse case result. The monochromatic case is discussed in Sect. III. Our purpose is not a numerical calculation of the transition rates, but an analysis of the position of the singularities they present in this ideal case. In the study of the electron distributions in the monochromatic case, one has to distinguish between the

”bare momentum” \mathbf{p}_2 (the momentum of the asymptotically free electron) and the ”dressed momentum” \mathbf{q}_2 of the scattered electron; these momenta are in biunivocal correspondence. We have found that the analytic part of this exploration is more easily done in terms of the dressed momenta. The electron distribution present δ -type singularities at particular values of the final dressed momentum $\mathbf{q}_2^{(N)}$, indexed by the positive integer N which is interpreted as the number of laser photons absorbed by the electron. We follow these singularities in the space of the polar coordinates $(|\mathbf{q}_2|, \theta_{q_2}, \phi_{q_2})$ of the vector \mathbf{q}_2 . The manifold of the singularities for a fixed N is a surface which may be closed or not. We find a subset of points on this surface at which the distribution has a particular type of singularity that influences the electron angular distribution. Then, we translate the results in terms of the bare momentum \mathbf{p}_2 of the electron and use them in the numerical illustration that concludes Sect. III. We find that, for not too high laser intensity, this type of representation is useful in understanding the distributions obtained with finite pulses. Section IV is devoted to the equations valid in the pulse case. The numerical results presented in Sect. V for two type of pulses reveal conditions in which the analysis done in the monochromatic case is useful.

In Appendices A and B we give details about the justification of some of the results presented in Sect. III concerning the monochromatic case.

II. THE THEORETICAL FRAMEWORK. GENERAL EXPRESSION FOR THE TRANSITION PROBABILITY

The general theoretical framework is the same as in [9], so not too many details will be given here. The same formalism is described in other recent publications [10–12].

The system investigated consists in an electron (charge $e < 0$, mass m) interacting with the quantized electromagnetic field describing the emitted photon and with a classical electromagnetic plane wave with the unit vector \mathbf{n}_1 in the direction of propagation and described by a vector potential

$$\mathbf{A}(\phi), \quad \phi = t - \mathbf{n}_1 \cdot \mathbf{r}/c = \frac{n_1 \cdot x}{c}, \quad (1)$$

where c is the velocity of the light and $n_1 \equiv (1, \mathbf{n}_1)$ is the notation for a four vector associated to the laser propagation direction. We take the z axis along $\mathbf{n}_1 \equiv \mathbf{e}_z$ and we

work with the vector potential

$$\mathbf{A}(\phi) = A_0 f(\phi) [\mathbf{e}_x \cos(\zeta/2) \sin(\omega_1 \phi) + \mathbf{e}_y \sin(\zeta/2) \cos(\omega_1 \phi)]. \quad (2)$$

This way the unit vectors \mathbf{e}_x and \mathbf{e}_y of the x and y axes are chosen along the axes of the ellipse associated with the state of polarization of the external field. The wave polarization is described by the parameter ζ ($\zeta = 0$ and π correspond to linear polarization, $\zeta = \pm\pi/2$ to circular polarization); in our numerical calculations only the case of circular polarization will be considered. In the *monochromatic case*, $f = 1$ and ω_1 is the laser frequency; in the case of a *laser pulse*, the function f is the pulse envelope, supposed to be significantly different from zero only in a finite interval $(\phi_{\text{in}}, \phi_{\text{f}})$, and ω_1 is the central frequency. The maximum amplitude reached by the electric field of the pulse is $\omega_1 A_0$ and the electromagnetic field intensity is characterized by the dimensionless parameter

$$\eta = \frac{|e| A_0}{mc}. \quad (3)$$

The formalism we use starts with the general definition of the transition amplitude between two states of the system (electron + quantized electromagnetic field + classical electromagnetic plane wave),

$$\mathcal{M}_{1 \rightarrow 2} = \lim_{t_2 \rightarrow \infty} \lim_{t_1 \rightarrow -\infty} \langle \Psi_2(t_2) | U(t_2, t_1) | \Psi_1(t_1) \rangle, \quad (4)$$

with U the evolution operator of the system. The initial and final states are products of free electron states of momenta \mathbf{p}_1 and \mathbf{p}_2 with, respectively, the vacuum state of the electromagnetic field and the one photon state of momentum \mathbf{k}_2 and polarization \mathbf{s}_2 . In contrast to [9], where a spinor with well determined momentum, normalized on an arbitrary volume V , was used for the initial state of the electron, now we describe formally the electron with a momentum \mathbf{p}_1 by a “wave-packet”,

$$\Psi_1(\mathbf{r}, t) = \int_{\mathbf{p}} \Phi(\mathbf{p}) \frac{e^{\frac{i}{\hbar}(\mathbf{p} \cdot \mathbf{r} - Et)}}{(2\pi\hbar)^{3/2}} \xi(p) d\mathbf{p}, \quad |\Phi(\mathbf{p})|^2 = \delta(\mathbf{p} - \mathbf{p}_1), \quad (5)$$

where $\xi(p)$ is a solution of Dirac equation $(\hat{p} - mc)\xi(p) = 0$ and it is normalized to 1 ($\xi^\dagger \xi = 1$), and $E = \sqrt{m^2 c^4 + c^2 \mathbf{p}^2}$. This procedure was used recently in [21] for a spinless particle.

The interaction of the electron with the quantized electromagnetic field, responsible for the photon emission, is treated in the first order of perturbation theory. The action of the

free evolution operator U_0 (describing only the electron in the classical electromagnetic plane wave) on the free states leads to the Volkov states for which we use the explicit expression in Eq. (B4) of [9], with V replaced by $(2\pi\hbar)^3$. In the following formulas we use the four-momenta p_1, p_2 of the initial, respectively final electron [$p_j \equiv (E_j/c, \mathbf{p}_j)$, $E_j = c\sqrt{m^2c^2 + \mathbf{p}_j^2}$, $j = 1, 2$] and k_2 of the photon.

The expression of the *transition probability* for the emission of a photon with the wave-vector $\mathbf{k}_2 \in d\mathbf{k}_2$ and a scattered electron with momentum $\mathbf{p}_2 \in d\mathbf{p}_2$, averaged over the initial spin of the electron and summed over the final spin, is :

$$d^4\Pi_{\text{unpol}} = \Pi_4(k_2, p_2) \delta(\mathbf{p}_{1\perp} - \mathbf{p}_{2\perp} - \hbar\mathbf{k}_{2\perp}) \delta[n_1 \cdot (p_1 - p_2 - \hbar k_2)] d\mathbf{k}_2 d\mathbf{p}_2, \quad (6)$$

where the subscript \perp is used to indicate the components orthogonal on the laser propagation direction \mathbf{n}_1 and the function Π_4 has the expression

$$\begin{aligned} \Pi_4(k_2, p_2) = & \frac{e_0^2}{4\pi^2} \frac{m^2c^5}{E_2(n_1 \cdot p_1)} \frac{1}{\hbar\omega_2} \left\{ |\mathcal{B}|^2 \left(-1 + \frac{(p_1 \cdot n_1)(p_2 \cdot k_2) + (p_1 \cdot k_2)(p_2 \cdot n_1)}{(mc)^2 k_2 \cdot n_1} \right) + \right. \\ & \left. \left(1 + \frac{(\hbar k_2 \cdot n_1)^2}{2(n_1 \cdot p_1)(n_1 \cdot p_2)} \right) \left[|\mathcal{A}|^2 - 2 \frac{(n_1 \cdot p_1)(n_1 \cdot p_2)}{(mc)\hbar k_2 \cdot n_1} \Re \left\{ \mathcal{B}^* \left(\frac{\mathcal{A} \cdot \mathbf{p}_1}{n_1 \cdot p_1} - \frac{\mathcal{A} \cdot \mathbf{p}_2}{n_1 \cdot p_2} \right) \right\} \right] \right\}, \quad (7) \end{aligned}$$

($e_0 = e/\sqrt{4\pi\epsilon_0}$). The external field dependence is contained in three one-dimensional integrals \mathcal{B} , \mathcal{A}_x and \mathcal{A}_y defined as

$$\mathcal{B}(2, 1) \equiv \int_{-\infty}^{\infty} d\phi \exp \left[-\frac{i}{\hbar} G(p_1, p_2, k_2; \phi) \right], \quad (8)$$

$$\mathcal{A}(2, 1) \equiv - \int_{-\infty}^{\infty} d\phi \frac{e\mathbf{A}(\phi)}{mc} \exp \left[-\frac{i}{\hbar} G(p_1, p_2, k_2; \phi) \right], \quad (9)$$

where the function $G(p_1, p_2, k_2; \phi)$ is

$$G(p_1, p_2, k_2; \phi) = \left[c \frac{\phi}{2} \tilde{n}_1 \cdot (p_1 - p_2 - \hbar k_2) + F(p_1; \phi) - F(p_2; \phi) \right], \quad (10)$$

$$F(p; \phi) = \frac{c}{2n_1 \cdot p} \int_{\phi_0}^{\phi} d\chi [e^2 \mathbf{A}^2(\chi) - 2e\mathbf{A}(\chi) \cdot \mathbf{p}], \quad (11)$$

with $\tilde{n}_1 \equiv (1, -\mathbf{n}_1)$. In the case of a pulse, where the vector potential is different from 0 for $\phi \in (\phi_{\text{in}}, \phi_{\text{f}})$, one has $\phi_0 = \phi_{\text{in}}$. In the monochromatic case the indefinite integral can be used, as the change of the value given to ϕ_0 leads only to the modification of a phase factor in the Volkov solution.

Finally, we remind here a classicality criterion presented several times in the literature (see, for example, [10, 13]): the scattering of the radiation can be treated in the framework of CED, if the ratio $(s_{\text{eff}} \hbar \omega_1 \gamma_1)/(m c^2 (1 + \eta^2))$, with γ_1 the Lorentz factor of the initial electron and s_{eff} the maximum number of laser photons absorbed, is small compared to 1. For $\eta \leq 1$, s_{eff} is of the order of unity; for $\eta \gg 1$, s_{eff} increases rapidly, proportional to η^3 , and the ratio becomes

$$y = \frac{\eta \hbar \omega_1 \gamma_1}{m c^2}. \quad (12)$$

If y becomes of the order of unity or larger, then the quantum behaviour sets in, and, as discussed before, one can expect to obtain a final electron distribution different from the initial one.

III. THE MONOCHROMATIC CASE

In the monochromatic case, as known for long time [1], the integrals $\mathcal{A}_x, \mathcal{A}_y$ and \mathcal{B} have analytic expressions as series of generalized Bessel functions. In these series each term contains an one-dimensional δ -function, as illustrated here by the integral \mathcal{A}_x ,

$$\mathcal{A}_x(2, 1) = \sum_{N=-\infty}^{\infty} A_x^{(N)} \delta[\tilde{n}_1 \cdot (q_1 + N \hbar k_1 - q_2 - \hbar k_2)]. \quad (13)$$

The four-momentum k_1 ,

$$k_1 \equiv (k_1^0, \mathbf{k}_1) = \frac{\omega_1}{c} n_1, \quad (14)$$

is interpreted as the momentum of a photon associated to the electromagnetic monochromatic plane wave. In Eq. (13) appears the dressed four-momentum q , a quantity met also in the description of the electron motion in classical theory, connected with the bare four-momentum p by

$$q = p + \frac{m U_P}{n_1 \cdot p} n_1, \quad U_P = \frac{e^2 A_0^2}{4 m}, \quad n_1 \cdot p = n_1 \cdot q. \quad (15)$$

Between the two 4-momenta q and p the correspondence is biunivocal, p can be expressed as a function of q as

$$p = q - \frac{m U_P}{n_1 \cdot q} n_1. \quad (16)$$

For a given four momentum p , the first component is $p_0 = E/c$ and the first component of q is $q_0 = W/c$, where

$$E = c \sqrt{\mathbf{p}^2 + m^2 c^2}, \quad W = c \sqrt{\mathbf{q}^2 + m_*^2 c^2}, \quad m_* = m \sqrt{1 + \frac{e^2 A_0^2}{2 m^2 c^2}}, \quad (17)$$

with m_* the dressed-mass, named also the shifted mass.

The use in the fully differential probability (6) of the integrals $\mathcal{A}(2, 1)$ and $\mathcal{B}(2, 1)$, as series of δ -functions similar to (13), gives an expression for $d^4\Pi_{\text{unpol}}$ from which, after standard manipulations, one extracts *the transition rate*, denoted $d^4\Gamma$. It has the structure

$$d^4\Gamma(\mathbf{p}_2, \mathbf{q}_2) = \sum_{N=1}^{\infty} \gamma_4^{(N)}(\mathbf{q}_2, \mathbf{k}_2) \delta(q_1 + N\hbar k_1 - q_2 - \hbar k_2) d\mathbf{q}_2 d\mathbf{k}_2, \quad (18)$$

i.e., $d^4\Gamma$ is a series of four-dimensional δ -functions with coefficients depending on the variables \mathbf{q}_2 and \mathbf{k}_2 . A term with fixed N in the previous expression is the contribution to the differential rate of the process in which N laser photons have been absorbed.

In the monochromatic case it is customary [24] to present these distributions as functions of \mathbf{q}_2 , but it is also possible to present them taking as variable \mathbf{p}_2 , using the relation

$$d\mathbf{q}_2 = \left(1 + \frac{mcU_P}{(p_2 \cdot n_1) E_2} \right) d\mathbf{p}_2, \quad (19)$$

with the ponderomotive potential U_P defined in (15).

In the following we shall suppose that in the "partial rates" $\gamma_4^{(N)}$ the connection between the momenta imposed by the δ -function was observed. In fact the product of four one-dimensional δ -functions leaves arbitrary only two of the six components of the three-dimensional final momenta \mathbf{q}_2 and \mathbf{k}_2 . Our purpose is not the evaluation of the partial rates, but the analysis of the implication of the conservation rules for each term with fixed N , in the case of the electron distribution. As we shall see in Sect. V, in appropriate conditions, connections are possible between the results of this analysis and the electron distributions in the pulsed wave case.

In order to get the differential rates describing the *electron energy and angular distributions* we have to integrate over the emitted photon momentum. This is a direct operation performed by three of the four δ -functions in each term and it imposes the following values to the emitted photon momentum

$$\hbar\tilde{\mathbf{k}}_2 = \mathbf{q}_1 - \mathbf{q}_2 + N\hbar\mathbf{k}_1. \quad (20)$$

The expression allowed for the frequency is $c\tilde{k}_2^0 \equiv c|\tilde{\mathbf{k}}_2|$. After the integration on \mathbf{k}_2 only an one-dimensional δ -function is left in each term of the series which represents the double differential rate $d^2\Gamma_e$ describing the scattered electron, in terms of the dressed momentum

\mathbf{q}_2 ,

$$d^2\Gamma_e = \sum_{N=1}^{\infty} \Gamma^{(N)}(\mathbf{q}_2) \delta \left[\frac{1}{m_*c} (q_2^0 + \hbar \tilde{k}_2^0 - q_1^0 - N \hbar k_1^0) \right] d\mathbf{q}_2, \quad (21)$$

with $\Gamma^{(N)}(\mathbf{q}_2) \equiv \gamma_4^{(N)}(\mathbf{q}_2, \tilde{\mathbf{k}}_2)/(m_*c\hbar^3)$.

In the following we emphasize some particularities of the electron distributions that come out from an analysis of the argument of the δ -function in (21).

A. Simultaneous detection of electron energy and direction

In the monochromatic case the final electron distribution is written as a series of δ -functions, as displayed by Eq. (21). We shall study the position of the singularities in the variables W_2 [or, equivalently, $|\mathbf{q}_2|$ related to W_2 by (17)], and $\hat{\mathbf{q}}_2$, the unit vector along the direction of the final dressed momentum \mathbf{q}_2 of polar angles θ_{q_2} and ϕ_{q_2} . It is convenient to introduce a new four-vector

$$Q_N = q_1 + N\hbar k_1 \equiv \left(\frac{\mathcal{E}_N}{c}, \mathbf{Q}_N \right), \quad \mathbf{Q}_N \equiv \mathbf{q}_1 + N\hbar \mathbf{k}_1, \quad \mathcal{E}_N \equiv W_1 + N\hbar\omega_1 \quad (22)$$

for which we have

$$Q_N^2 = (m_*c)^2 + 2N\hbar k_1 \cdot q_1. \quad (23)$$

We emphasize that for given laser intensity and fixed N , the four-vector Q_N is well determined only by the values of q_1 and k_1 . In the reference frame described at the beginning of Sect. II, we denote by θ_N and ϕ_N the polar angles of the vector \mathbf{Q}_N , and by $\alpha_N \in [0, \pi]$ the angle between the momentum \mathbf{q}_2 and the vector \mathbf{Q}_N . With (22) the argument of the δ -function in a term with *fixed* N in (21) is

$$F_N(\mathbf{q}_2) \equiv \frac{1}{m_*c} (q_2^0 + \hbar \tilde{k}_2^0 - Q_N^0) = \frac{1}{m_*c^2} (W_2 + c |\mathbf{Q}_N - \mathbf{q}_2| - \mathcal{E}_N). \quad (24)$$

The equation

$$F_N(\mathbf{q}_2) = 0. \quad (25)$$

determines the position of the singularities in the space of the variables W_2 (or $|\mathbf{q}_2|$) and $\hat{\mathbf{q}}_2$. The condition (25), for $N \geq 1$ defines a family of surfaces in the space $(|\mathbf{q}_2|, \theta_{q_2}, \phi_{q_2})$; the differential rate (21) has a δ -type singularity along these surfaces and is zero otherwise.

Before going in more detail, we draw attention to an approximate symmetry property of F_N , valid in the case $\eta \sim 1$, when the number of terms which gives practically non-negligible

contribution to the electron distribution is limited to a value N_{max} of the order of unity. In this case it makes sense to analyze the condition (25) only for $N \leq N_{max}$. If, in addition, $\gamma_1 \gg 1$ and the direction of the bare momentum \mathbf{p}_1 is not too close to \mathbf{n}_1 , then, the angle α_N between \mathbf{q}_2 and \mathbf{Q}_N is approximately equal to the angle between \mathbf{q}_2 and \mathbf{p}_1 . As a consequence, the solutions of Eq. (25) have, with a very good approximation, a rotational symmetry with respect to the direction of the incident electron direction.

We remark also that because in the regime ($\gamma_1 \gg \eta \sim 1$) the dressed momentum \mathbf{q}_2 is very close to \mathbf{p}_2 , the two distributions, one expressed in terms of the variables of \mathbf{q}_2 , the other in terms of \mathbf{p}_2 , are almost identical.

In order to obtain the energy distribution or the angular distribution of the scattered electrons, one needs to integrate the double differential distribution (21) over the parameters that are not observed, by writing the δ -function in a way convenient for each distribution.

For the *angular distribution* we need the relation:

$$\delta(F_N(\mathbf{q}_2)) = \sum_{\text{sol}} \frac{\delta(X - X^{\text{sol}})}{\left| \frac{\partial F_N}{\partial X} \right|} = \frac{1}{m_*c} \sum_{\text{sol}} \frac{q_2^0 |\mathbf{Q}_N - \mathbf{q}_2|}{|\mathbf{Q}_N| \sqrt{\cos^2 \alpha_N - C_N}} \delta(X - X^{\text{sol}}), \quad (26)$$

which is based on the solutions (A9) and (A10) of Eq. (25) for the unknown $X \equiv |\mathbf{q}_2|/(m_*c)$; the quantity C_N is defined in (A2). By the generic summation index 'sol', we understand the (one or two) solutions acceptable at fixed N (see details in Appendix A). When this expression is replaced in (21), it displays the position of the singularities in X at fixed direction of \mathbf{q}_2 .

For $\frac{\partial F_N}{\partial X} = 0$ the expression in (26) for $\delta(F_N(\mathbf{q}_2))$ is not valid. In the following, we work with $\cos \alpha_N < \sqrt{C_N}$ and after obtaining the angular distributions, we take the limit $\cos \alpha_N = \sqrt{C_N}$. As shown further, the singularity present in the double differential distribution (21) influences the angular distribution of the electrons, obtained after integration on the scattered electron energy.

To prepare (21) for the calculation of the *energy distribution*, we have to find the polar angles of \mathbf{q}_2 that are solutions of (25) at fixed $|\mathbf{q}_2|$. The equation (A4) gives us, for any X in the interval (A5), the unique solution for $\cos \alpha_N$, denoted by $Y(X)$ (see Appendix A). From it we derive the possible values for the polar angles of \mathbf{q}_2 by solving the equation

$$\cos \theta_N \cos \theta_{q_2} + \sin \theta_N \sin \theta_{q_2} \cos(\phi_{q_2} - \phi_N) = Y(X), \quad (27)$$

considering as the unknown variables one of the two angle θ_{q_2} or ϕ_{q_2} , with fixed $Y(X)$.

Simple particular cases are collinear and head-on collisions [$\sin \theta_N = 0$, $\cos \theta_N = \pm 1$], when Eq. (27) is an equation for θ_{q_2} only, with the solution $\cos \theta_{q_2} = \sigma_N Y(X)$ with $\sigma_N = \text{sgn}(\cos \theta_N)$. In this case we write the δ -function in (21) as

$$\delta(F_N(\mathbf{q}_2)) = m_* c \frac{|\mathbf{Q}_N - \mathbf{q}_2|}{|\mathbf{q}_2| |\mathbf{Q}_N|} \delta(\cos \theta_{q_2} - \sigma_N Y(X)), \quad \sin \theta_N = 0. \quad (28)$$

The cases $\theta_N \neq 0, \pi$ are more complicated since both angles θ_{q_2} and ϕ_{q_2} appear in Eq. (27). One possibility is to solve Eq. (27) for the unknown ϕ_{q_2} , keeping as parameter θ_{q_2} . As shown in Appendix B, Eq. (27) has two solutions,

$$\phi^{\text{sol}} = \phi_N \pm \Phi_0, \quad \Phi_0 = \arccos \left[\frac{Y(X) - \cos \theta_N \cos \theta_{q_2}}{\sin \theta_N \sin \theta_{q_2}} \right]. \quad (29)$$

if θ_{q_2} obeys the condition

$$\cos \theta_{q_2} \in [\cos(\theta_N + \alpha_N), \cos(\theta_N - \alpha_N)]. \quad (30)$$

This condition defines an angular range that we denote by \mathcal{I}_θ . We emphasize that in the present context the value taken by the angle α_N depends on $|\mathbf{q}_2|$, being expressed as $\alpha_N = \arccos(Y(X))$. Finally, the procedure leads to the expression of δ -function in (21)

$$\delta(F_N(\mathbf{q}_2)) = m_* c \sum_{\text{sol}} \frac{|\mathbf{Q}_N - \mathbf{q}_2|}{|\mathbf{q}_2| |\mathbf{Q}_N|} \frac{1}{|\sin \theta_N \sin \theta_{q_2} \sin \Phi_0|} \delta(\phi_{q_2} - \phi^{\text{sol}}), \quad \sin \theta_N \neq 0. \quad (31)$$

With this expression of $\delta(F_N)$ the distribution (21) displays the position of the singularities in ϕ_{q_2} at fixed θ_{q_2} and $|\mathbf{q}_2|$.

If we choose to solve the equation (27) for the unknown θ_{q_2} with ϕ_{q_2} as a parameter, the solutions are more complicated. With the notation $u_{q_2} = \cos \theta_{q_2}$, one finds (for details, see Appendix B) two possible solutions:

$$u_{q_2}^{(\pm)} = \frac{1}{s_N} \left(Y(X) \cos \theta_N \pm \sin \theta_N |\cos(\phi_{q_2} - \phi_N)| \sqrt{s_N - Y^2(X)} \right). \quad (32)$$

$$s_N \equiv \cos^2 \theta_N + \sin^2 \theta_N \cos^2(\phi_{q_2} - \phi_N). \quad (33)$$

Depending on the initial conditions and on the value of ϕ_{q_2} , one or both solutions are acceptable, namely:

i) for $Y^2(X) \leq \cos^2 \theta_N$, only one solution is acceptable for any value of ϕ_{q_2} : $u_{q_2}^{(+)}$, if $\cos \theta_N \cos(\phi_{q_2} - \phi_N) < 0$, and $u_{q_2}^{(-)}$, if $\cos \theta_N \cos(\phi_{q_2} - \phi_N) > 0$,

ii) for $\cos^2 \theta_N < Y^2(X) \leq 1$, both solutions $u_{q_2}^{(\pm)}$, are acceptable, but the domain of ϕ_{q_2} is reduced to $\phi_{q_2} \in [\phi_N - \phi_0, \phi_N + \phi_0]$ if $Y(X) > 0$ and to $\phi_{q_2} \in [\pi + \phi_N - \phi_0, \pi + \phi_N + \phi_0]$ if $Y(X) < 0$, where $\phi_0 = \arccos \sqrt{(Y^2(X) - \cos^2 \alpha_N) / \sin^2 \alpha_N} \in (0, \pi/2)$.

The δ -function in (21) is written now as

$$\delta(F_N(|\mathbf{q}_2|; u_{q_2}, \phi_{q_2})) = m_* c \sum_{\text{sol}} \frac{|\mathbf{Q}_N - \mathbf{q}_2| \sqrt{1 - (u_{q_2}^{(\text{sol})})^2} \delta(u_{q_2} - u_{q_2}^{(\text{sol})})}{2 |\mathbf{Q}_N| |\mathbf{q}_2| \sqrt{s_N - Y^2(X)}}. \quad (34)$$

It gives the position of the singularities in θ_{q_2} at fixed ϕ_{q_2} and $|\mathbf{q}_2|$.

B. Angular distribution of electrons

We get the angular distribution of electrons using the expression (26) in the distribution (21) and integrating over $|\mathbf{q}_2| = (m_* c) X$, with the result

$$\frac{d\Gamma_e}{d\Omega_{q_2}} = \sum_{N \geq 1} \sum_{\text{sol}} \frac{|\mathbf{q}_2|^2 W_2 |\mathbf{Q}_N - \mathbf{q}_2|}{c |\mathbf{Q}_N|} \frac{\Gamma^{(N)}(\mathbf{q}_2)}{\sqrt{\cos^2 \alpha_N - C_N}} \Big|_{|\mathbf{q}_2| = m_* c X^{\text{sol}}} \equiv \sum_N \Gamma_{e, \text{ang}}^{(N)}. \quad (35)$$

The substitution rule indicated above means that the modulus of \mathbf{q}_2 must be replaced everywhere by $(m_* c) X^{\text{sol}}$, with X^{sol} given by Eq. (A9) or (A10).

Based on the results in Sect. III A, Appendix A and some more details given in Appendix B, we mention here the main features of the angular distribution. We describe the situation of a term $\Gamma_{e, \text{ang}}^{(N)}$, with a fixed value of N . If, for that N , we are in the case I, when $C_N < 0$, [C_N defined in (A2)] there is one solution X^{sol} [Eq. (A9)] for any $\cos \alpha_N \in [0, \pi]$, i.e. for any direction of the scattered electron, and the term $\Gamma_{e, \text{ang}}^{(N)}$ in the sum (35) is finite. If, for the considered N , we are in the case II, when $0 < C_N < 1$, then, there are two solutions X^{sol} [Eq. (A10)] for any direction α_N obeying the condition $\cos \alpha_N \leq \sqrt{C_N}$. For $\cos \alpha_N = \sqrt{C_N}$, the two solutions X_{\pm} in (A10) coalesce and the corresponding $\Gamma_{e, \text{ang}}^{(N)}$ has a singularity. The condition $\cos \alpha_N \leq \sqrt{C_N}$, determining the possible scattering angles for a given N in the case II, can be expressed in terms of polar angles of the electron in the form $\{\theta_{q_2}, \phi_{q_2}\} \in \mathcal{D}(C_N)$. The explicit expression of the domain $\mathcal{D}(C_N)$ is deduced in Appendix B.

C. Energy distribution of electrons

The energy distribution is obtained by integrating the fully differential distribution (21) over the electron directions determined by the angles θ_{q_2} and ϕ_{q_2} .

For collinear and head-on collisions, using (28), the integral over θ_{q_2} is performed directly and the energy distribution becomes

$$\frac{d\Gamma_e}{dW_2} = \frac{m_*}{c} \sum_{N \geq 1} \int_0^{2\pi} d\phi_{q_2} \frac{W_2 |\mathbf{Q}_N - \mathbf{q}_2|}{|\mathbf{Q}_N|} \Gamma^{(N)}(\mathbf{q}_2) \Big|_{\theta_{q_2} = \theta_{\text{sol}}} = \sum_{N \geq 1} \Gamma_{e,W}^{(N)}, \quad \sin \theta_N = 0, \quad (36)$$

where $\theta_{\text{sol}} = \arccos(Y(|\mathbf{q}_2|/(m_*c)))$, if $\sigma_N = 1$, and $\theta_{\text{sol}} = \pi - \arccos(Y(|\mathbf{q}_2|/(m_*c)))$ if $\sigma_N = -1$, with $Y(|\mathbf{q}_2|/(m_*c))$ calculated according to (A4).

For other initial configurations, it is convenient to use in (21) the expression (31) of the δ -function and, as a consequence, in the calculation of the energy distribution the integral over ϕ_{q_2} is performed directly. After that, for the integral on θ_{q_2} that has to be done numerically, the domain of integration reduces to the interval \mathcal{I}_θ defined by the condition (30). The final result reads:

$$\frac{d\Gamma_e}{dW_2} = \frac{m_*}{c} \sum_{N \geq 1} \sum_{\text{sol}} \int_{\mathcal{I}_\theta} \frac{d\theta_{q_2}}{\sin \theta_N \sin \Phi_0} \frac{W_2 |\mathbf{Q}_N - \mathbf{q}_2|}{|\mathbf{Q}_N|} \Gamma^{(N)}(\mathbf{q}_2) \Big|_{\phi_{q_2} = \phi^{\text{sol}}} = \sum_{N \geq 1} \Gamma_{e,W}^{(N)} \quad (37)$$

with ϕ^{sol} and Φ_0 given by (29).

D. An example

We illustrate the previous analysis by an example. We have seen that the δ -function in the multiple differential distribution (18) imposes the restriction (25) on the vector \mathbf{q}_2 and we have described the position of the singularities in terms of $(W_2, \theta_{q_2}, \phi_{q_2})$. As mentioned in Sect. III A the analysis can be converted in terms of the bare momentum \mathbf{p}_2 . In this case we think of surfaces in the space $(E_2, \theta_{p_2}, \phi_{p_2})$ on which the singularities are localized. In the example that follows we shall present graphs with the curves giving the position of the singularities in the plane (E_2, θ_{p_2}) at fixed $\phi_{p_2} = \phi_{p_1}$.

We choose the case of an electron of energy $E_1 = 46.6$ GeV scattered by a circularly polarized monochromatic wave with the frequency $\omega_1 = 0.043$ a.u. (1.17 eV) and the field intensity $I = 4.4 \times 10^{17}$ W/cm² ($\eta = 0.6$); these conditions are close to those in the SLAC experiment, in which the detection of NLCS was achieved. We consider two cases for the initial direction of the electron: (a) $\theta_{p_1} = 0.9\pi$, close to the value used at SLAC, and (b) $\theta_{p_1} = 0.5\pi$ (orthogonal geometry), with $\phi_{p_1} = 0$ in both cases. For these initial conditions we have $n_1 \cdot q_1 > m_*c$ and we are in the case II (defined in III.A) for values of N up to

$\approx 10^6$; this value is much larger than the maximum value of N contributing to the electron distribution at the intensity considered, which is of the order of ten.

We describe the position of the δ -type singularities in the double differential distribution (21) based on Eq. (34), giving some details valid in our particular case, $\phi_{p_1} = \phi_{p_2} = 0$, using as variables the bare energy E_{p_2} and polar angle θ_{p_2} . In the present discussion, preceding Fig. 1, we have in mind only low values of N (of the order of ten), for which, as we have mentioned before, we are in the case I. In the particular case $\phi_{p_2} = \phi_{p_1} = 0$ we have chosen, for any X in the interval (A5) (i.e. for any energy W_2 in (A8)) the two acceptable solutions of Eq. (27), given by Eq. (32), reduce to $\theta_{q_2} = \theta_N \pm \arccos Y(X)$ which coalesce for $Y(X) = 1$, i.e. at the ends $W_2 = W_a$ and $W_2 = W_b$ of the interval. The maximum domain of variation for the angles is given by the condition

$$\theta_{q_2} \in [\theta_{q,A} = \theta_N - \arccos Y_{\min}, \theta_{q,B} = \theta_N + \arccos Y_{\min}], \quad (38)$$

with Y_{\min} given by (A6). This domain can be transcribed in terms of bare energy and scattering angle, using the relation

$$\theta_{qA,B} \rightarrow \theta_{pA,B} = \arccos \left(\frac{|\mathbf{q}_2| \cos \theta_{qA,B} - m^2 c^2 \eta^2 / (4n_1 \cdot q_2)}{\sqrt{(W_2 - m^2 c^3 \eta^2 / (4n_1 \cdot q_2))^2 / c^2 - m^2 c^2}} \right) \quad (39)$$

for the angles and Eq. (17) for the energy.

In the regime discussed here ($\gamma \gg \eta \sim 1$), \mathbf{q}_1 and \mathbf{q}_2 are very close to the corresponding bare momenta \mathbf{p}_1 and respectively \mathbf{p}_2 , so the results in the plane (E_{p_2}, θ_{p_2}) are practically identical at the graphical level to those in (W_2, θ_{q_2}) ; in particular, we have $W_{a,b} \approx E_{a,b}$ and $\theta_{pA,B} \approx \theta_{qA,B}$. Another particularity is that the upper limits of the intervals $W_b(N) \approx E_b(N)$, defined in (A8), are almost independent of N and approximately equal to the initial electron energy E_1 ; the lower limits, however, are significantly dependent of N . Then, the energy of the final electron in the process in which N photons are absorbed takes values in an interval $E_2 \in (E_a(N), E_1)$ with $E_a(N) < E_a(N - 1)$. The successive values $E_a(N)$ are named *thresholds* of the energy spectrum.

In Figures 1 (a) and (b), for the two values of θ_{p_1} we have chosen for the direction of the incident electron, we display in the plane (E_{p_2}, θ_{p_2}) the curves that represent the solutions of Eq. (25) for N taking values from 1 to 11. The coordinate along the y axis is $\delta\theta$, defined as $\delta\theta \equiv \theta_{p_2} - \theta_{p_1}$; the good symmetry of the two figures with respect to the value $\delta\theta = 0$ is a consequence of the rotational symmetry around the direction of \mathbf{p}_1 mentioned

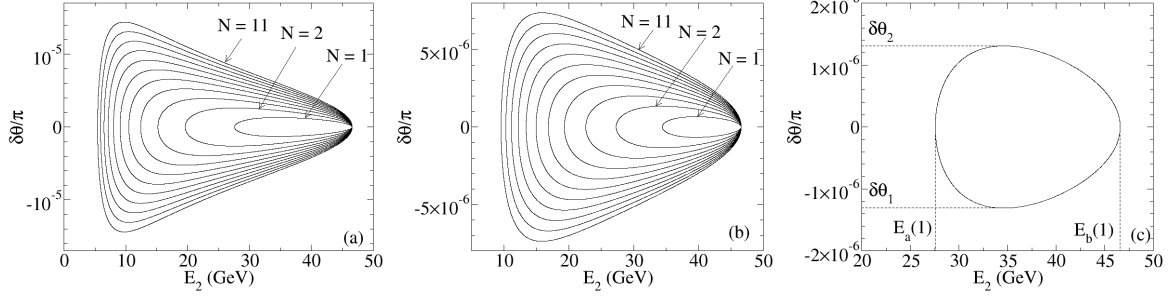


FIG. 1: Position of the first eleven lines in the plane (E_2, θ_2) for $E_1 = 46.6$ GeV, $\eta = 0.6$, circular polarization and two directions of the incident electron: (a) $\theta_{p_1} = 0.9\pi$ and (b) $\theta_{p_1} = 0.5\pi$; (c): detailed view of (a) for $N = 1$.

in Sect. III A. The results show that $\delta\theta$ takes very small values for all N , i.e. the final electron direction is very close to the initial one for all the cases represented ($N \leq 11$). On the other hand, the energies E_2 are spread till relatively small values. The interpretation of these results is that in case (a) the electron can lose up to 45% of its initial energy in the process in which only one photon is absorbed ($N = 1$), and up to 85% for $N = 11$. In case (b), when the initial electron incident orthogonal on the laser pulse direction, the angular distribution is more compressed towards small angles and it is also compressed in the region of larger final energies. As, according to the conservation laws, the energy lost by the electron is converted in the energy of the emitted photon, this means that this case is less efficient for energy conversion.

In Fig. 1 (c) is presented only the curve with $N = 1$ from the case (a). The limits $E_a(1)$ and $E_b(1)$ of the domain in energy that gives contribution to the spectrum, obtained from Eq. (A8) using Eq. (17), are marked on the graph; for any $E_2 \in (E_a(1), E_b(1))$ there are two angles θ_{q_2} for which the equation (25) is verified, they become a double root for $E_2 = E_a(1)$ and $E_2 = E_b(1)$. As discussed after Eq. (39) the value $E_a(1)$ corresponds to the threshold of one photon absorption in the energy spectrum. The domain of angles θ_{p_2} that contribute to the angular distribution for $N = 1$ is the interval $(\theta_{p_1} + \delta\theta_1, \theta_{p_1} + \delta\theta_2)$; within this interval there are two solutions E_2 of Eq. (25), which coalesce for $\theta_{p_2} = \theta_{p_1} + \delta\theta_1$ or $\theta_{p_2} = \theta_{p_1} + \delta\theta_2$.

Another aspect worth to be discussed is which would be the dependence of the type of curves represented in Fig. 1 (a) and (b) on the laser intensity. One feature to be considered is the increase of the maximum number of photons that can be absorbed in the process with

the laser intensity. The other feature is that, at fixed N and q_1 , when the laser intensity increases the curves tend to become closer to each other, i.e. the domain in which the energy of the final electron can take values shrinks. This process can be understood using the concept of “dressed mass”: when the laser intensity increases the electron becomes heavier, and consequently its recoil at fixed number of photons absorbed decreases.

IV. THE PLANE WAVE PULSE

We consider now the more realistic model of a pulsed plane wave, going back to Eqs. (6) and (7). In the pulse case, the integral \mathcal{B} is expressed in terms of convergent integrals, using Eq.(30) of [9] (see also, [14] for an alternative approach).

Now, as only three δ -functions appear in (6), only three conditions are imposed to the six variables \mathbf{p}_2 and \mathbf{q}_2 , namely

$$\mathbf{p}_{1\perp} - \mathbf{p}_{2\perp} - \hbar\mathbf{k}_{2\perp} = 0, \quad n_1 \cdot (p_1 - p_2 - \hbar k_2) = 0. \quad (40)$$

In order to get the one-particle (electron or photon) distribution, the differential distribution (6) is integrated over the momentum of the that is not detected using the conservation rules (40). The integration over the orthogonal components of the momenta is performed directly using the δ function, so from (40) we get the replacement rules to be used in (7),

$$\mathbf{p}_{2\perp} \rightarrow \tilde{\mathbf{p}}_{2\perp} = \mathbf{p}_{1\perp} - \hbar\mathbf{k}_{2\perp} \quad (41)$$

for the integration over the orthogonal component of the *photon* momentum, and respectively,

$$\hbar\mathbf{k}_{2\perp} \rightarrow \tilde{\hbar\mathbf{k}}_{2\perp} = \mathbf{p}_{1\perp} - \mathbf{p}_{2\perp} \quad (42)$$

for the integration over the orthogonal component of the *electron* momentum. The integration over the third component requires some further calculation, due to the fact that the second relation in (40) contains a combination of energy and momenta. We present the results in both cases. Using the adequate relations from the following ones,

$$\delta[n \cdot (p_1 - p_2 - \hbar k_2)] = \frac{\tilde{E}_2}{cn_1 \cdot (p_1 - \hbar k_2)} \delta(p_{2z} - \tilde{p}_{2z}) = \frac{\hbar\tilde{\omega}_2}{cn_1 \cdot (p_1 - p_2)} \delta(k_{2z} - \tilde{k}_{2z}), \quad (43)$$

with

$$\tilde{p}_{2z} = \frac{(mc)^2 + (\mathbf{p}_{1\perp} - \hbar\mathbf{k}_{2\perp})^2}{2n_1 \cdot (p_1 - \hbar k_2)} - \frac{n_1 \cdot (p_1 - \hbar k_2)}{2}, \quad \tilde{\hbar k}_{2z} = \frac{(\mathbf{p}_{1\perp} - \mathbf{p}_{2\perp})^2}{2n_1 \cdot (p_1 - p_2)} - \frac{n_1 \cdot (p_1 - p_2)}{2}, \quad (44)$$

and

$$\frac{\tilde{E}_2}{c} = \frac{(mc)^2 + (\mathbf{p}_{1\perp} - \hbar\mathbf{k}_{2\perp})^2}{2n_1 \cdot (p_1 - \hbar k_2)} + \frac{n_1 \cdot (p_1 - \hbar k_2)}{2}, \quad \frac{\hbar\tilde{\omega}_2}{c} = \frac{(\mathbf{p}_{1\perp} - \mathbf{p}_{2\perp})^2}{2n_1 \cdot (p_1 - p_2)} + \frac{n_1 \cdot (p_1 - p_2)}{2}, \quad (45)$$

one obtains the two one-particle (photon or electron) distributions,

$$d^2\Gamma_\gamma = \frac{\tilde{E}_2}{cn_1 \cdot \tilde{p}_2} \frac{\omega_2^2}{c^3} \Pi_4(k_2, \tilde{p}_2) d\omega_2 d\Omega_{k_2}, \quad (46)$$

$$d^2\Gamma_e = \frac{E_2}{cn_1 \cdot \hbar\tilde{k}_2} \frac{\tilde{\omega}_2 |\mathbf{p}_2|}{\hbar^2 c^2} \Pi_4(\tilde{k}_2, p_2) dE_2 d\Omega_{p_2}. \quad (47)$$

The attribute *unpolarized* was omitted.

NB. The quantity denoted here by \tilde{k}_2 is different from that defined in (20) and used in Sect. III, as it comes out from a different conservation rule.

The structure of the previous two distributions, using each in a specific way the same function Π_4 implies the possibility of connections between the two distributions, as it will be mentioned at the end of Sect. VB.

V. NUMERICAL RESULTS

We consider two type of pulses: i) a pulse with a finite duration, of almost rectangular shape, with the envelope $f(\phi)$ in Eq. (2) constant on a region of length equal to a multiple N_c of periods of the carrier, and two very short smooth wings; we shall name this pulse “quasimonochromatic”, ii) a pulse without a constant region, consisting in two wings of variable length. We shall see that the first type of pulse, if N_c is large enough, leads to results similar to those predicted by the monochromatic approximation, which explain the adopted terminology. The contribution to the scattering probability of the wings of the pulse is very small compared to the contribution of the flat central region, still these smooth wings are required in order to ensure the continuity of the vector potential and of its derivative. The results obtained with the second pulse are considerably different from the monochromatic ones.

In Fig. 2 is represented the vector potential \mathbf{A} as a function on ϕ/T for the two pulses mentioned before. The rectangular portion of the pulse in (a) has the length of $N_c=8$ periods of the carrier. In the case (b) we have chosen a \cos^2 envelope, the total length of the pulse corresponds to a number N_t of periods of the carrier equal to 10. In both cases

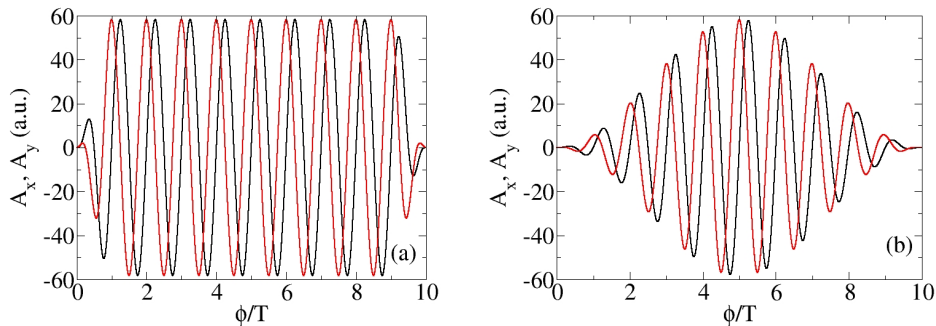


FIG. 2: (Color online) The components A_x and A_y of the vector potential for a rectangular pulse with $N_c = 8$ cycles (a) and for a \cos^2 pulse with $N_t = 10$ cycles.

the parameter η is 0.6 (the value used in the SLAC experiment). In all numerical examples presented here we choose the laser central frequency $\omega_1 = 0.043$ a.u. (1.17 eV) and circular polarization.

A. Effect of the pulse shape

We have calculated the electron double differential probability distribution $d^2\Gamma_e/dE_2d\Omega_{p_2}$ for the conditions of the SLAC experiment ($\omega_1 = 0.043$ a.u., $\eta = 0.6$, $E_1 = 46.6$ GeV) and for the two pulses represented in Fig. 2.

In Fig. 3 (a) and (b), we present results in a logarithmic color scale in the same coordinates as those in Fig. 1 (E_2 , $\delta\theta = \theta_{p_2} - \theta_{p_1}$). The case considered is $\phi_{p_2} = \phi_{p_1} = 0$, as in Fig. 1. Due to the very good symmetry of the results with respect to $\delta\theta = 0$, remarked also in the discussion of the monochromatic case (Sect IIID), only the values $\delta\theta < 0$ are presented. In both figures one can see a series of maxima located on curves with the same shape as those presented in Fig. 1 in the monochromatic case. Notice that in Fig. 1 both $\delta\theta < 0$ and $\delta\theta >$ are represented. For the intensity we consider, with a relatively low value, only the first 11 maxima are visible. The difference between the two cases is that, while for the rectangular pulse the maxima are very sharp, and have a fine substructure, for the \cos^2 pulse the main maxima and their subpeaks become wider and smooth.

In Fig. 3 (c) are represented the energy distributions $d\Gamma_e/dE_2$, for the rectangular pulse (full black line) and for the \cos^2 pulse (dashed red line). The two distributions are similar, having a “ladder-like” structure, with successive shoulders which can be understood based

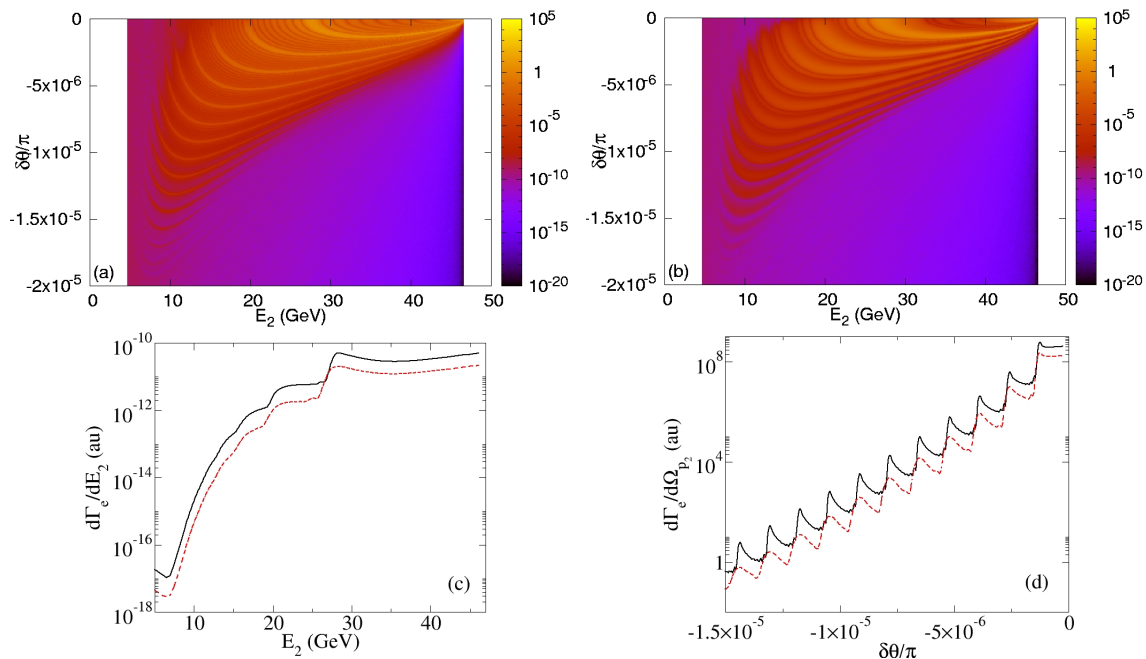


FIG. 3: (Color online) (a): Electron probability distribution $\frac{d^2\Gamma_e}{dE_2 d\Omega_{p_2}}$ for the conditions of SLAC experiment and for a rectangular pulse; (b): the same as in (a), but for a \cos^2 pulse; (c): energy probability distribution for the two pulses; (d): angular probability distribution for the two pulses. Black (full) lines refer to the case of rectangular pulse, and red (dashed) lines are for the \cos^2 pulse.

on the monochromatic limit: their positions coincide with the thresholds $E_a(N) \approx W_a(N)$ in Eq. (A8); the upper limits $E_b(N)$ are almost independent of N and approximately equal to the initial electron energy E_1 . The first interval at the right in Fig. 3 (c) covers the region $E_2 \in (E_a(1) \approx 27.6 \text{ GeV}, E_1)$ and can be interpreted as the sum of contributions of the processes in which any number of photons $N \geq 1$ can be absorbed. The next step, the region $E_2 \in (E_a(2) \approx 18. \text{ GeV}, E_a(1) \approx 27.6 \text{ GeV})$, is the contribution of the processes with $N \geq 2$, as $N = 1$ does not contribute anymore and so on. The fact that the values of the successive steps decrease very fast (note the logarithmic scale) is due to the relatively small value of η , still close to the perturbative regime. The figure 3 (c) is similar to Fig. 4 in [5], calculated there in the monochromatic approximation.

The angular distribution $d\Gamma_e/d\Omega_{p_2}$ for $\phi_{p_2} = \phi_{p_1} = 0$ and variable θ_{p_2} for the same two pulses as before is presented in Fig. 3 (d). Here one can see again the same “ladder-like” structure, but, unlike in the case of the energy distribution, there is a sharp maximum at the left end of each step. These maxima are the correspondent of the singularities of the

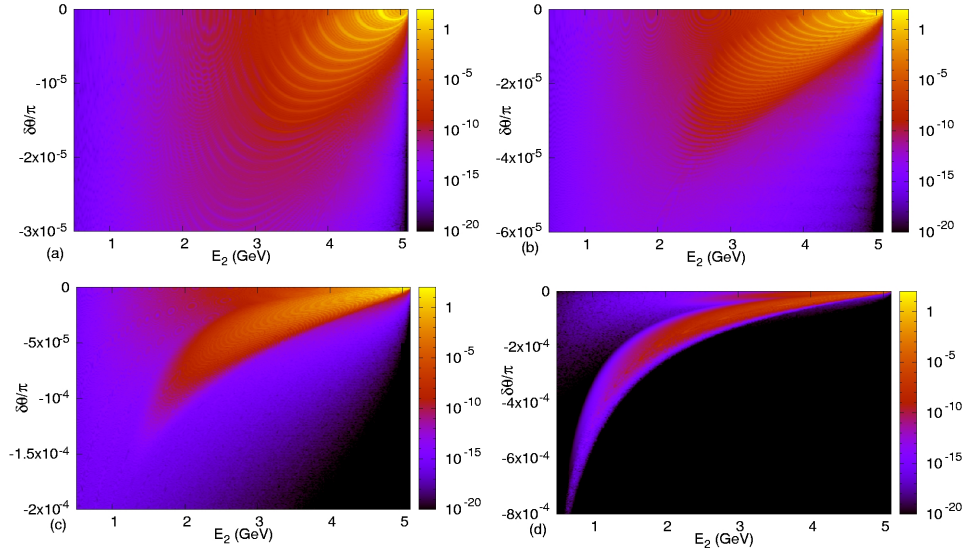


FIG. 4: (Color online) Electron probability distribution $\frac{d^2\Gamma_e}{dE_2 d\Omega_{p_2}}$ as a function of γ_2 and $\delta\theta$ for head-on collision, initial electron energy $E_1 = 10^4 mc^2$, and four values of the field intensity: $\eta = 0.5$ (a), $\eta = 1$ (b), $\eta = 2$ (c), $\eta = 5$ (d).

angular distribution existent in the monochromatic case [see Sect. III C] and are localized at $\delta\theta_{pA}(N)$ given by (39), as presented in the example III.D. As expected, they are much better defined for the rectangular pulse than for the \cos^2 pulse.

B. Effect of the field intensity

We illustrate now the influence of the laser intensity on the double differential distribution (47) of the electron.

In Fig. 4 we consider the case of a rectangular pulse with $N_c = 6T$ and a head-on collision ($\theta_{p_1} = \pi$) with the electron having the initial Lorentz factor $\gamma_1 = 10^4$. As in the previous subsection, we represent the probability distribution $\frac{d^2\Gamma_e}{dE_2 d\Omega_{p_2}}$ in the plane $(\gamma_2, \delta\theta = \theta_{p_2} - \theta_{p_1})$. We remind that since we are in the case of head-on collisions and the laser is circularly polarized, the electron spectrum is symmetric with respect to rotations around the z axis, i.e. it does not depend on the angle ϕ_{p_2} . We have chosen four values of the parameter η : 0.5, 1, 2 and 4. For the first two values the spectra present a series of maxima localized along curves whose shape and distribution is that of the lines predicted in the monochromatic case (see Fig. 1). However, when η increases, the successive peaks become so close to each other

that they start to overlap, tending to form a smooth continuum, so we hardly distinguish them in Fig.4 (b) and not at all in Figs. 4(c) and (d). This behaviour is in agreement with the discussion at the end of Sect. III. In the last two cases we remark another interesting feature: for $\eta \geq 2$ the distribution does not cover uniformly the plane $(\gamma_2, \delta\theta)$ but only a small region, with a well defined shape.

The behaviour found in Figs. 4 (c) and (d) can be understood in correlation with the *photon distribution*. In [25] it was shown that in the case of an ultrarelativistic electron and for large values of η , the photons are emitted only in a well defined, very small domain of angles; although in the cited paper only the CED formalism is used, it can be shown that the conclusion concerning the photon distribution are valid also in the quantum case. For a rectangular pulse, as that considered here, and for head-on collisions, the emitted radiation has a continuous spectrum, extended from $\omega_2 = 0$ and up to a maximum value Ω_M , and it is emitted practically at a constant angle θ_0 , symmetrically around the z axis, $\theta_{k_2} \in (\theta_0 - \delta, \theta_0 + \delta)$, $\delta \ll 1$. In terms of photon momentum, this means that the function $\Pi_4(k_2, \tilde{p}_2)$ in (6) is non-negligible only for \mathbf{k}_2 along the directions of the unit vectors $\mathbf{e}_0 \equiv (\sin \theta_0 \cos \phi, \sin \theta_0 \sin \phi, \cos \theta_0)$, with $\phi \in (0, 2\pi)$; when expressed in terms of electron momentum, according to the conservation rules (42), (45), this condition leads to the particular shapes present in Fig. 4 (c) and (d). The correlation between the electron and photon distributions needs further investigation.

C. Effect of the initial electron energy

We present in Fig. 5 the electron energy distribution $d\Gamma/dE_2$ for the case of a head-on collision, $\eta = 5$, and for four values of the initial electron energy: $\gamma_1 = 10$ ($E_1 = 5.11$ MeV) in full line, $\gamma_1 = 10^2$ ($E_1 = 51.1$ MeV) in dashed line, $\gamma_1 = 10^3$ ($E_1 = 511$ MeV) in dotted line, $\gamma_1 = 10^4$ ($E_1 = 5.11$ GeV) in dash-dotted line. The laser pulse is rectangular, with $N_c = 10$ cycles. The values of the classicality parameter (12) in the four cases are, respectively, $y = 1.1 \times 10^{-4}$, 1.1×10^{-3} , 1.1×10^{-2} , 1.1×10^{-1} .

The coordinate along the x axis is chosen as $1 - E_2/E_1$ and the results are presented in a log-log scale. For the lowest value considered for the incident electron energy, the energy distribution decreases very fast with the ratio E_2/E_1 : practically the entire distribution is contained in the interval $E_2 \in (0.992E_1, E_1)$ which is an indication of the classicality of the

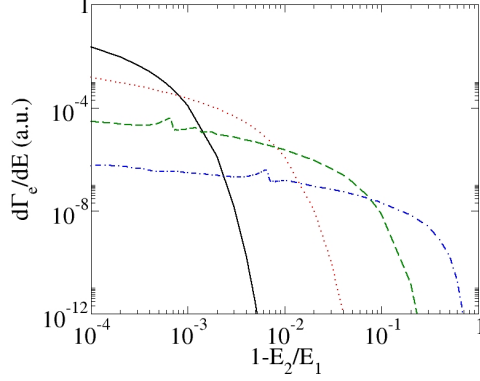


FIG. 5: (Color online) The energy distribution $d\Gamma_e/dE_2$ for $\eta = 5$ and four values of the initial electron energy: $E_1 = 5.1$ MeV (full black line), $E_1 = 51.1$ MeV (dotted red line), $E_1 = 511$ MeV (dashed green line), $E_1 = 5.1$ GeV (dot-dashed blue line) .

process. With the increase of the initial electron energy, the energy spectrum is extended towards lower values of E_2/E_1 , and its slope is much lower, as an indication of the onset of the quantum behaviour; for the largest value of the incident electron energy considered ($\gamma_1 = 10^4$, $E_1 = 5.11$ GeV) the electron can lose up to 90% of its energy.

The small peaks visible in the energy distribution for $\gamma_1 = 10^3$ and $\gamma_1 = 10^4$ correspond to the limit $E_a(1) \approx W_a(1)$ [Eq. (A8)] of the energy range in which one photon absorption contributes. For the other two values of γ_1 these points are located at values of $1 - E_2/E_1 < 10^{-4}$, not represented in our figure. The presence of this one photon peak can be explained using the analogy with the electron behaviour in the monochromatic case, based on conservation laws valid in that case: for E_2 very close to E_1 the electron direction changes very little, and the photon is emitted at an angle extremely small with respect to the initial electron direction, i.e. $\theta_{k_2} \approx \pi$. It is known for a long time [26] that for this geometry the terms with high N in the radiation spectrum are suppressed, i.e. only the first few terms contribute to the total rate, even if η is relatively large, and successive thresholds are visible in the electron distributions. For smaller values of E_2 the angular distribution widens, and many values of N contribute to the total rate, i.e. the typical behaviour for large η sets in: the successive maxima become broader and overlap, giving rise to a smooth continuum.

VI. CONCLUSIONS

The aim of our theoretical study of NLCS was a first description of several features of the scattered electron distributions in the case of a pulsed electromagnetic wave. We have identified two possible guides for a qualitative understanding of the electron distribution: the monochromatic limit and the emitted radiation pattern. Which one is useful, if any, depends on several parameters: pulse shape (duration and intensity) and initial electron momentum. While the role and condition of applicability of the first guide was identified in the present study, the connection with the emitted radiation spectrum requires further investigation.

Appendix A: The solutions of equation (25)

In order to present the properties of the solutions of the equation (25), we use the notations (22) and define a set of dimensionless quantities:

$$u_N = \frac{Q_N^0}{m_*c}, \quad v_N = \frac{|\mathbf{Q}_N|}{m_*c}, \quad X = \frac{|\mathbf{q}_2|}{m_*c} \geq 0, \quad (\text{A1})$$

and we use the notations

$$\cos \alpha_N = Y \in [-1, 1], \quad C_N = \frac{4u_N^2 - (u_N^2 - v_N^2 + 1)^2}{4v_N^2}. \quad (\text{A2})$$

It is useful to emphasize that while u_N, v_N and C_N are determined by the initial conditions, X and Y are variables, connected with the final momentum \mathbf{q}_2 , which is subject to the condition (25).

Analyzing the equation (25), we have found that we have to distinguish between two cases:

Case I: $u_N - v_N > 1$, when $C_N < 0$,

Case II: $u_N - v_N < 1$, when $0 < C_N < 1$.

We have found that if the momentum of the incident electron fulfills the condition $n_1 \cdot q_1 - m_*c > 0$, we are in the case I for $N\hbar\omega_1 > m_*c \frac{W_1 - m_*c^2}{n_1 \cdot q_1 - m_*c}$ and in the case II for $N\hbar\omega_1 < m_*c \frac{W_1 - m_*c^2}{n_1 \cdot q_1 - m_*c}$. If $n_1 \cdot q_1 - m_*c < 0$, we are in the case I for any value of N .

The numerical examples presented in this paper (Sect. IIID and IV) refer to the case of head-on or nearly head-on collision of a very energetic electron with a laser pulse of

moderate intensity ($\gamma_1 \gg \eta \sim 1$). For these initial conditions we have $n_1 \cdot q_1 > m_* c$, and we are in the case II for all values of N which gives non-negligible contribution to the electron distribution.

When written explicitly, the function F_N [Eq. (24)] is a function of the two unknowns X and Y , defined in (A1) and (A2), respectively. This way Eq. (25) becomes

$$F_N(X, Y) \equiv \sqrt{X^2 + 1} - \sqrt{X^2 + v_N^2 - 2XYv_N} - u_N = 0. \quad (\text{A3})$$

It can be easily solved as an equation for Y , with the parameter X , leading to the expression

$$Y(X) = \frac{2u_N \sqrt{X^2 + 1} - (u_N^2 + 1 - v_N^2)}{2Xv_N}. \quad (\text{A4})$$

The properties of the function $Y(X)$ are different in the two cases mentioned before:

Case I ($u_N > v_N + 1$): Y increases monotonously with X and the condition $|Y(X)| \leq 1$ leads to a domain of acceptable values of X

$$X \in \left[\left| \frac{u_N - v_N}{2} - \frac{1}{2(u_N - v_N)} \right|, \frac{u_N + v_N}{2} - \frac{1}{2(u_N + v_N)} \right] \quad (\text{A5})$$

Case II ($u_N < v_N + 1$): Y has a minimum

$$Y_{\min} = \sqrt{C_N} \in (0, 1), \quad (\text{A6})$$

reached for

$$X_d = \frac{\sqrt{4u_N^2 - (u_N^2 + 1 - v_N^2)^2}}{u_N^2 - v_N^2 + 1}. \quad (\text{A7})$$

The condition $|Y(X)| \leq 1$ leads to the same domain (A5) of values for X as in the case I. When expressed in terms of energy of the dressed electrons, the interval (A5) is $W_2 \in [W_a, W_b]$ with

$$W_a(N) = \mathcal{E}_N - \frac{N\hbar\omega_1}{\mathcal{E}_N/c - |\mathbf{Q}_N|} n_1 \cdot q_1, \quad W_b(N) = \mathcal{E}_N - \frac{N\hbar\omega_1}{\mathcal{E}_N/c + |\mathbf{Q}_N|} n_1 \cdot q_1. \quad (\text{A8})$$

Going the other way around, i.e. solving the equation (25) for the unknown X as function of Y , we find:

i) only one solution in the case I, namely

$$X_+(Y) = \frac{v_N Y (u_N^2 - v_N^2 + 1) + 2u_N v_N \sqrt{Y^2 - C_N}}{2(u_N^2 - v_N^2 Y^2)} \quad (\text{A9})$$

for any $Y \in [-1, 1]$,

ii) two values for X in case II,

$$X_{\pm}(Y) = \frac{v_N Y (u_N^2 - v_N^2 + 1) \pm 2u_N v_N \sqrt{Y^2 - C_N}}{2(u_N^2 - v_N^2 Y^2)} \quad (\text{A10})$$

for $Y \in [Y_{\min}, 1]$. At $Y = Y_{\min}$ the two solutions X_{\pm} coalesce to the value X_d in Eq. (A7).

In conclusion we have established the equations that describe the position of the singularities brought by the δ -functions in (21) in terms of the variables X or Y .

Appendix B: Study of the solutions of Eq. (27)

With the notations

$$u_{q_2} = \cos \theta_{q_2}, \quad y = \cos \theta_N, \quad \delta\phi = \phi_{q_2} - \phi_N, \quad (\text{B1})$$

Eq. (27) for $\cos \delta\phi$ becomes

$$Y = u_{q_2} y - \sqrt{1 - u_{q_2}^2} \sqrt{1 - y^2} \cos \delta\phi. \quad (\text{B2})$$

The parameters u_{q_2}, y, Y are subject to the conditions $|Y|, |y|, |u_{q_2}| \leq 1$. The solution

$$\delta\phi = \pm \arccos \rho(u_{q_2}), \quad \rho(u_{q_2}) = \frac{Y - u_{q_2} y}{\sqrt{1 - u_{q_2}^2} \sqrt{1 - y^2}}. \quad (\text{B3})$$

is acceptable, if ρ has the modulus less than unit. From the expression of its derivative

$$\frac{d\rho}{du_{q_2}} = \frac{Y u_{q_2} - y}{(1 - u_{q_2}^2)^{3/2} \sqrt{1 - y^2}} \quad (\text{B4})$$

we see that for $|Y| < |y|$, ρ is a monotonic function, taking values between -1 and 1 when u_{q_2} takes values in the interval

$$u_{q_2} \in [u_{q_2, \min} = yY - \sqrt{1 - y^2} \sqrt{1 - Y^2}, u_{q_2, \max} = yY + \sqrt{1 - y^2} \sqrt{1 - Y^2}]. \quad (\text{B5})$$

In terms of angles this condition becomes Eq. (30). If $|Y| > |y|$, then $\rho(u_{q_2})$ has an extremum equal to $\text{sgn}(Y) \sqrt{\frac{Y^2 - y^2}{1 - y^2}}$ for $x = Y/y$; the condition $|\rho(u_{q_2})| < 1$ leads to the same interval (B5).

When equation (27) is solved for the unknown u_{q_2} at fixed ϕ_{q_2} , we obtain: For $|Y| > |y|$, there are two solutions

$$u_{q_2}^{(\pm)} = \frac{Y y \pm \sqrt{1 - y^2} |\cos \delta\phi| \sqrt{y^2 + (1 - y^2) \rho^2 - Y^2}}{y} + (1 - y^2) \cos^2 \delta\phi \quad (\text{B6})$$

acceptable only for $\cos \delta\phi \in [\sqrt{\frac{Y^2-y^2}{1-y^2}}, 1]$ if $Y > 0$, and for $\cos \delta\phi \in [-1, -\sqrt{\frac{Y^2-y^2}{1-y^2}}]$ if $Y < 0$. For $|Y| < |y|$ there is only one solution for any $\phi \in [-\pi, \pi]$: $u_{q_2}^{(-)}$, if $y \cos \delta\phi > 0$, or $u_{q_2}^{(+)}$ if $y \cos \delta\phi < 0$.

Now we can write explicitly the domain $\mathcal{D}(C_N)$ introduced in Section III A, defined by the condition $\cos \alpha_N \leq \sqrt{C_N}$. We refer to the solutions (B6), assuming that in their expression Y was replaced by $\sqrt{C_N} > 0$. Then the domain $\mathcal{D}(C_N)$ can be described by:

$\phi_{q_2} \in [\phi_N - \phi_0, \phi_N + \phi_0]$, $\cos \theta_{q_2} \in [u_{q_2}^{(-)}, u_{q_2}^{(+)})]$, where $\phi_0 = \arccos \sqrt{\frac{C_N - \cos^2 \theta_N}{\sin^2 \theta_N}}$, for $|\cos \theta_N| \leq \sqrt{C_N}$;

$\phi_{q_2} \in [\phi_N - \pi, \phi_N + \pi]$, $\cos \theta_{q_2} \in [u_{q_2}^{(-)}, 1]$ if $\cos(\phi_{q_2} - \phi_N) > 0$ and $\cos \theta_{q_2} \in [u_{q_2}^{(+)}, 1]$ if $\cos(\phi_{q_2} - \phi_N) > 0$, for $\cos \theta_N > \sqrt{C_N}$;

$\phi_{q_2} \in [\phi_N - \pi, \phi_N + \pi]$, $\cos \theta_{q_2} \in [-1, u_{q_2}^{(-)}]$ if $\cos(\phi_{q_2} - \phi_N) > 0$ and $\cos \theta_{q_2} \in [-1, u_{q_2}^{(+)})]$ if $\cos(\phi_{q_2} - \phi_N) > 0$ for $\cos \theta_N < -\sqrt{C_N}$.

Acknowledgments

This work was supported by CNCSIS-UEFISCSU, project number 488 PNII-IDEI 1909/2008. M.B. acknowledges the support of the strategic grant POSDRU/89/1.5/S/58852, Project ‘‘Postdoctoral programme for training scientific researchers’’ cofinanced by the European Social Found within the Sectorial Operational Program Human Resources Development 2007-2013. V.D. thanks A. Ilderton for a useful discussion about the description of the initial state of the electron.

-
- [1] N. B. Narozhnyi, A.I. Nikishov, and V. I. Ritus, JETP **47**, 930 (1964) [Sov. Phys. JETP **20**, 622 (1965)].
 - [2] Y. I. Salamin, S. X. Hu, K. Z. Hatsagortsyan and C. H. Keitel, Physics Reports **427**, 41 (2006).
 - [3] F. Ehlotzky, K. Krajewska and J. Z. Kaminski, Rep. Prog. Phys. **72**, 046401 (2009).
 - [4] C. Bula *et al.*, Phys. Rev. Lett **76**, 3116 (1996).
 - [5] C. Bamber *et al.*, Phys. Rev. D **60**, 092004 (1999).

- [6] A. Di Piazza, C. Müller, K. Z. Hatsagortzyan and C. H. Keitel, arXiv:1111.3886v2 [hep-ph], accepted by Reviews of Modern Physics.
- [7] A. Di Piazza, K. Z. Hatsagortzyan, and C. H. Keitel, Phys. Rev. Lett. **105**, 220403 (2010).
- [8] I. V. Sokolov *et al.*, Phys. Rev. E **81**, 036412 (2010).
- [9] M. Boca and V. Florescu, Phys. Rev. A **80**, 053403 (2009).
- [10] T. Heinzl, D. Seipt, and B. Kämpfer, Phys. Rev. A **81**, 022125 (2010).
- [11] D. Seipt and B. Kämpfer, Phys. Rev. A **83**, 022101 (2011).
- [12] F. Mackenroth and A. Di Piazza, Phys. Rev. A **83**, 032106 (2011).
- [13] F. Mackenroth, A. Di Piazza, and C. H. Keitel, Phys. Rev. Lett. **105**, 063903 (2010).
- [14] A. Ilderton, Phys. Rev. Lett. **106**, 020404 (2011).
- [15] T. Heinzl, A. Ilderton, M. Marklund, Phys. Lett. B **692**, 250 (2010).
- [16] J. Gao, J. Phys. B: At. Mol. Opt. Phys. **39**, 1345 (2006).
- [17] A. L. Galkin *et al.*, Contrib. Plasma Phys. **49**, 593 (2009).
- [18] M. Babzien *et al.* Phys. Rev. Lett. **96**, 054802 (2006).
- [19] The White Book of ELI Nuclear Physics, Bucharest-Magurele, Romania, <http://www.elinp.ro/documents/ELI-NP-WhiteBook.pdf>.
- [20] A. Di Piazza, C. Müller, K. Z. Hatsagortzyan, and C. H. Keitel, arXiv:1111.3886v1 [hep-ph].
- [21] J. P. Corson, J. Peatross, C. Muller, K. Z. Hatsagortzyan, Phys. Rev. A **84**, 053831 (2011).
- [22] J. P. Corson and J. Peatross, Phys. Rev. A **84**, 053832 (2011).
- [23] M. Boca, V. Dinu and V. Florescu, Nucl. Instrum. Meth. B, **279**, 12 (2012).
- [24] Y. I. Salamin and F. H. M. Faisal, Phys. Rev. A **54**, 4383 (1996).
- [25] M. Boca and A. Oprea, Phys. Scr. **83**, 055404 (2011).
- [26] E. Esarey, S. K. Ride, P. Sprangle, Phys. Rev. E **48**, 3003 (1993).